Editors' Suggestion

Topological Thermal Hall Conductance of Even-Denominator Fractional States

Arup Kumar Paul,[1] Priya Tiwari,[1] Ron Melcer,[2] Vladimir Umansky,[1] and Moty Heiblum[1,*]
[1]Braun Center for Submicron Research, Department of Condensed Matter Physics, Weizmann Institute of Science, Rehovot 7610001, Israel
[2]Qedma Quantum Computing, Tel Aviv, Israel

(Received 14 February 2024; accepted 12 July 2024; published 16 August 2024)

The even-denominator fractional quantum Hall (FQH) states $\nu = 5/2$ and $\nu = 7/2$ have been long predicted to host non-Abelian quasiparticles. Their present energy-carrying neutral modes are hidden from customary conductance measurements and thus motivate thermal transport measurements, which are sensitive to all energy-carrying modes. While past "two-terminal" thermal conductance ($k_{2t}T$) measurements already proved the non-Abelian nature of the $\nu = 5/2$ FQH state, they might have been prone to a lack of thermal equilibration among the counterpropagating edge modes. Here, we report a novel thermal Hall conductance measurement of the $\nu = 5/2$ and $\nu = 7/2$ states, being insensitive to equilibration among edge modes. We verify the state's non-Abelian nature, with both states supporting a single upstream Majorana edge mode (hence, a particle-hole Pfaffian order). While current numerical works predict a different topological order, this contribution should motivate further theoretical work.

DOI: 10.1103/PhysRevLett.133.076601

Introduction—The search for quantum states that host non-Abelian quasiparticles (QPs), localized or propagating, intensified in the past few years, stemming from their unique characteristics and potential to serve as robust qubits in a noisy environment. Among several proposed implementations in the quantum Hall (QH) effect regime, even-denominator fractional states, such as the $\nu = 5/2$ and $\nu = 7/2$, are the leading candidates [1–12] with numerical calculations predicting an anti-Pfaffian (A-Pf) topological order [3,4]. This order supports a fractional downstream "charged mode" (in addition to downstream integer modes) and three upstream Majorana modes [2,7–17].

The $\nu = 5/2$ state has been studied extensively in the experimental realm. Earlier tunneling measurements pointed at various possible states, such as the A-Pf order [10,18,19] or different Abelian and non-Abelian orders [10,20]. However, more recent heat transport and shot noise measurements observed a "particle-hole Pfaffian" (PH-Pf) order [21–23]. The published works include measurements of (i) the two-terminal thermal conductance coefficient k_{2t} for all participating edge modes (two integers and fractions) [21]; (ii) k_{2t} for the isolated fractional channel (fractional charged and Majorana) [22]; and (iii) shot noise, testing the chirality of the isolated fractional channel [23]. The observed PH-Pf order differs from the A-Pf by supporting a single upstream Majorana mode (central charge, $c = -1/2$) [21,22]. The less explored $\nu = 7/2$ state is also expected to be non-Abelian [13–17]; however, its topological order was not established.

The "two-terminal" thermal conductance measurement [24,25] relies on a small floating Ohmic contact ("source"), with a known power being dissipated in it. The equilibrium temperature (T_H) of the source and k_{2t} are related to the net power (J_{2t}) that leaves the contact by

$$J_{2t} = 0.5k_{2t}(T_H^2 - T_0^2), \tag{1}$$

where T_0 is the ground temperature. For a single ballistic chiral Abelian mode, the thermal conductance ($G_{th} = dJ_{2t}/dT_H$) is quantized to $k_{2t}T = k_0T$, with $k_0 = \pi^2k_B^2/3h$, T temperature, and k_B and h are Boltzmann and Planck constants, respectively [26,27]. In quantum Hall states featuring both downstream and upstream edge modes, each with respective thermal conductances k_dT and k_uT, the net thermally equilibrated thermal conductance is $k_{2t}T = (k_d - k_u)T$. However, if the edge modes do not interact, then $k_{2t}T = (k_d + k_u)T$. Consequently, partial thermal equilibration can lead to any value between the two extremes of k_{2t} [28,29]. For example, in the $\nu = 5/2$ state, if an existing Majorana mode (with thermal conductance $k_0T/2$ [5,30–34]) will not interact, the two-terminal thermal conductance would increase by k_0T. Such a lack of equilibration might create the impression of the fully equilibrated PH-Pf order ($k_{2t} = 2.5k_0$) [35–41], while the true order is A-Pf (with equilibrated $k_{2t} = 1.5k_0$).

To mitigate the ambiguity arising from partial or no equilibration, we utilize a new measurement configuration that directly determines the topological thermal Hall conductance coefficient k_{xy}, of the $\nu = 5/2$ and $\nu = 7/2$ states [42,43]. This method involves separately measuring downstream and upstream heat flows (J_{down} and J_{up}) to

*Contact author: moty.heiblum@weizmann.ac.il

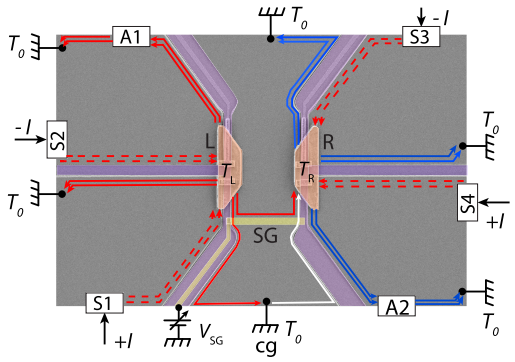

FIG. 1. The device and measurement setup: An SEM image of the device showing the floating contacts (orange), L (with temperature T_L), and R (with temperature T_R), the continuous side gate, SG (yellow, charged by V_{SG}), and the mesa arms (gray) defined by etching grooves (purple) in the GaAs. The arrowed lines represent the QH edge modes. Red dashed arrows show current-carrying edge modes (injected from contacts S1 and S2 or S3 and S4) that heat the floating contacts. Solid red and blue arrows represent the outgoing edge modes from contacts L and R, respectively, and they terminate at cold ground contacts connected to the dilution mixing chamber plate at base temperature T_0. The white arrow represents edge modes originating from cg A1 and A2 are amplifier contacts.

determine the coefficients k_d and k_u, ultimately yielding $k_{xy} = k_d - k_u$, which represents the topological order of the states [42,43].

Device and setup—The devices under test (shown in a false color SEM image in Fig. 1) were fabricated in a two-dimensional electron gas (2DEG) confined in a GaAs-AlGaAs heterostructure, with short-period superlattice (SPSL) type doping [44,45]. The 2DEG mobility $\sim 9.1 \times 10^6$ cm^2/V.s and density $\sim 2.9 \times 10^{11}$ cm^{-2}, are measured at 4.2 K in the dark.

The QH responses around the two states of interest, measured in a Hall bar, are shown in Supplemental Material-1 [46]. The tested devices (Fig. 1) consist of two identical floating Ohmic contacts, denoted by L (left) and R (right), each with an area of ~ 49 μm^2. Both contacts are covered with ~ 25 nm thick dielectric HfO_2 followed by a grounded thin metallic layer, which increases the contact capacitance and thus suppresses the charging energy [47,48]. The 2DEG (gray) under each floating contact is grooved (purple), thus "forcing" the incident current to enter the contacts [42,43]. Contacts L and R are separated by 10 μm (or 30 μm) of the intermediate 2DEG bulk. A side gate (SG, at the lower part of the intermediate bulk), when "pinched," guides the edge modes from L to R. When the SG is not biased, the chiral modes flow to the ground. Partial biasing of the SG directs chosen edge modes to the ground. Contacts L and R are also attached to two separate long mesa arms (~ 120 μm long each), with two current sourcing contacts (S1 and S2 or S3 and S4), amplifier contacts (A1 and A2), and cold grounds (cg) maintained at base temperature T_0 (Fig. 1). The amplifiers amplify the Johnson-Nyquist (JN) noise carried by edge modes (solid red and blue arrows) emanating from the floating contacts, facilitating the determination of the contact's temperature (refer to Supplemental Material-2 [46] for details) [42].

Each of the floating contacts is heated with a known power supplied by equal and opposite dc currents ($+I$ and $-I$) emanating from contacts S1 and S2 (for contact L) or S3 and S4 (for contact R). Each floating contact's potential remains zero, thus eliminating possible emanating shot noise and assuring that the outgoing edge modes carry only the JN noise. Under these conditions, the dissipating power is $P_d = I^2R$, with $R = h/\nu e^2$ the QH resistance. During measurements, one of the floating contacts is heated and acts as the temperature source (S) (see Supplemental Material [46], Fig. 2). The second floating contact is heated by the arrival power (carried by the edge modes and the bulk), thus acting as a power meter (PM). The increased PM temperature is "translated" (via a calibration process) to the arrival power from S (see Supplemental Material [46], Fig. 3) [42,43]. In the "downstream configuration," the floating contact L plays the role of the source while the floating contact R plays the PM role. In the "upstream configuration," the functions of L and R are interchanged.

We now briefly review the method of obtaining the topological thermal Hall conductance. The arriving downstream heat flow to the PM, $J_{\rm down}$, and the exiting heat from it, $J_{\rm out} = J_e + J_\gamma$ (J_e via edge modes, and J_γ via phonons) leads to net dissipated power in the PM with an equilibrium temperature $T_{\rm PM}$. This temperature is converted back to the arriving power, $J_{\rm down}$, via a separate heating process by a known power (as described above and also in Supplemental Material-2 [46]). The same procedure is applied when the upstream heat flow, $J_{\rm up}$, is measured by interchanging the heated and the absorbing contacts (L and R). The topological thermal conductance coefficient k_{xy} is determined from $J_{\rm down}$ and $J_{\rm up}$, using,

$$J_{\rm down} - J_{\rm up} = \frac{(k_d - k_u)}{2}(T^2 - T_0^2) = \frac{k_{xy}}{2}(T^2 - T_0^2), \qquad (2)$$

where T is the source (contact L for downstream and contact R for upstream) temperature [42]. It is important to stress that thermal equilibration between modes, or lack of it, as well as the contributions of the bulk or due to edge reconstruction, are eliminated by the subtraction process of $J_{\rm down} - J_{\rm up}$ [42,43]. However, the energy loss of the "down" and "up" propagating modes, not necessarily being equal, cannot be recovered. Hence, the L-R separation is kept short.

Results—We first test the configuration at the well-understood filling $\nu = 2$, performing the measurements at the conductance plateau's center ($B = 6$ T) on a device with a L-R separation of 10 μm. Figure 2(a) shows the measurement configuration with a fully pinched SG gate

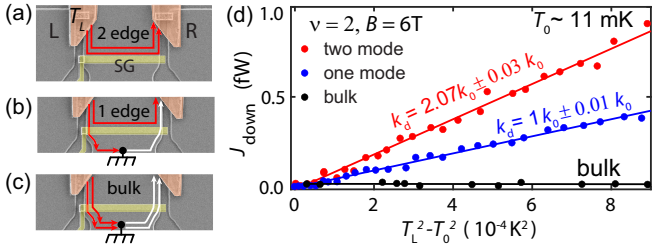

FIG. 2. Thermal conductance of $\nu = 2$: For downstream heat flow, contact L acts as the source, and contact R acts as the PM. (a) Configuration for downstream heat flow measurement with two edge modes (red arrows) carrying heat from L to R ($V_{SG} = -2$ V). (b) Configuration for the inner edge mode reaching contact R, while the outer edge mode is diverted to ground ($V_{SG} = -0.85$ V). (c) Configuration for bulk heat conduction with all the edge modes diverted to the ground ($V_{SG} = 0$ V). The white arrows represent edge modes starting from the ground. (d) Downstream heat flow J_{down} arrives at contact R and heats the contact. The J_{down} is plotted as a function of $T_L^2 - T_0^2$ ($T_0 \sim 11$ mK, electron temperature). The red, blue, and black colors correspond to heat conduction by two modes, one mode, and only the bulk, respectively. Solid lines are the linear fits to the data.

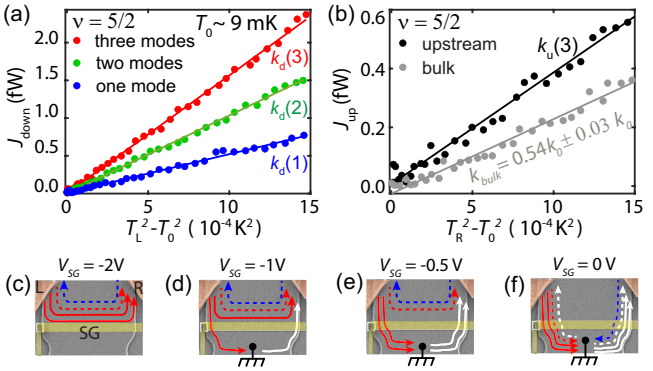

FIG. 3. Thermal conductance of $\nu = 5/2$: (a) Downstream heat flow J_{down} that leaves the heated contact L and reaches contact R vs $T_L^2 - T_0^2$ ($T_0 \sim 9$ mK, electron temperature). The red, green, and blue data points are for all edge modes (two integers and the innermost fractional mode), two inner modes (the inner integer mode and the fractional mode), and only the fractional mode, respectively. The downstream heat conductance coefficients $k_d(N = 3, 2, 1)$ are determined from the linear fittings shown by the solid lines and are given in Table I. (b) Upstream heat flow J_{up} measured by changing the roles of L and R with all modes participating (for fully pinched gate SG, $N = 3$) is plotted as a function of $T_R^2 - T_0^2$ (in black). The gray dots are for bulk heat transport when SG is fully open. (c)–(f) Different configurations of edge modes propagation between L and R: (c) Fully pinched SG ($V_{SG} = -2$ V), (d) and (e) Partially pinched SG with one ($V_{SG} = -1$ V) and two ($V_{SG} = -0.52$ V) edge modes diverted to ground. (f) Fully open SG ($V_{SG} = 0$ V). The arrows indicate edge modes: solid red for downstream integer modes, dashed red for downstream fractional mode, and blue dashed arrow for upstream modes. White arrows show edge modes emanating from the ground.

($V_{SG} = -2$ V), with two downstream edge modes leaving contact L (source) and reaching contact R (PM). Increasing the gate voltage to $V_{SG} = -0.85$ V (and to 0 V) enables the outer (and also the inner) modes to reach the ground as shown in Fig. 2(b) [and Fig. 2(c)]. Supplemental Material-3 [46] shows gate transmittance as a function of V_{SG} for the studied filling factors. Figure 2(d) shows the dependence of the (calibrated) incoming power J_{down} (reaching contact R) as a function of $T_L^2 - T_0^2$ ($T_0 \sim 11$ mK), where T_L is the temperature of contact L. The red, blue, and black dots correspond to downstream heat flow by two modes plus the bulk, one mode plus the bulk, and only the bulk ($V_{SG} = 0$ V), respectively. With Eq. (1), we find $k_d = 2.07k_0 \pm 0.03k_0$ for two propagating edge modes and $k_d = 1k_0 \pm 0.01k_0$ for a single edge mode. The heat flow through the bulk and the upstream heat flow are both negligibly small; hence, $k_{xy}(\nu = 2) \approxeq 2k_0$, as expected. To assess the impact of bulk's heat conductance, we also measured k_{xy}, away from the center of the $\nu = 2$ plateau (at 5.6 T) (see Supplemental Material-4 [46]). Here, despite having finite bulk heat conduction, we find similar values for k_{xy}, thus reassuring our method's effectiveness in determining the topological order of the states.

Having established the method's effectiveness, we now focus on the even-denominator states. Starting with the $\nu = 5/2$ state, Fig. 3(a) shows the J_{down} vs $T_L^2 - T_0^2$ ($T_0 \sim 9$ mK) plots measured at the center of $\nu = 5/2$ plateau (B ~ 4.64 T) for different SG voltages (refer to Supplemental Material-3 [46]). Figure 3(b) shows the J_{up} vs $T_R^2 - T_0^2$ plots for fully pinched SG (all edge mode participating) and of the bulk conduction when SG is fully transparent (see Supplemental Material-5 [46] for partially closed SG). Here, T_R is the temperature of contact R. Figures 3(c)–3(f) show the edge mode configurations between the two floating contacts with different SG voltages. The solid and dashed red arrows in these figures represent the downstream integer and the 1/2 fractional-edge mode, respectively. The blue arrows represent the upstream edge modes. For fully pinched SG (at $V_{SG} = -2$ V), all the edge modes move between the floating contacts [Fig. 3(c)]. The outermost integer modes are directed to the ground, with the outer at $V_{SG} = -1$ V [Fig. 3(d)] and the inner at $V_{SG} - 0.52$ V [Fig. 3(e)], leaving only the fractional modes (red and blue dashed arrows) propagating between the floating contacts. Finally, with the SG fully open [Fig. 3(f)], all the edge modes end up in the ground. Table I outlines the thermal conductance derived from the plots in Figs. 3(a) and 3(b). Here, the coefficients $k_d(N)$ and $k_u(N)$ represent downstream and upstream thermal conductance coefficients, respectively, for N number of downstream charged modes (integer and fractional) (Supplemental Material-3 [46]). Accordingly, the topological thermal Hall conductance coefficient is

TABLE I. Summary of measured downstream and upstream thermal conductance coefficients $k_d(N)$ and $k_u(N)$ and topological thermal Hall conductance coefficient $k_{xy}(N)$ as a function of the number of downstream charged edge modes (N) between the floating contacts L and R for the $\nu = 5/2$ and $\nu = 7/2$ states. k_{bulk} is the bulk thermal conductance.

ν	N	$k_d(N)$	$k_u(N)$	$k_{xy}(N)$	k_{bulk}
5/2	All modes, $N = 3$	$k_d(3) = 3.3k_0 \pm 0.05k_0$		$k_{xy}(3) = 2.5k_0 \pm 0.07k_0$	
	Inner modes, $N = 2$	$k_d(2) = 2.19k_0 \pm 0.03k_0$	$\sim 0.8k_0 \pm 0.02k_0$	$k_{xy}(2) = 1.39k_0 \pm 0.05k_0$	$\sim 0.54k_0 \pm 0.03k_0$
	Innermost fractional modes, $N = 1$	$k_d(1) = 1.09k_0 \pm 0.02k_0$		$k_{xy}(1) = 0.29k_0 \pm 0.04k_0$	
7/2	All modes, $N = 4$	$k_d(4) = 4k_0 \pm 0.05k_0$		$k_{xy}(4) = 3.48k_0 \pm 0.07k_0$	
	Inner modes, $N = 3$	$k_d(3) = 2.92k_0 \pm 0.07k_0$	$\sim 0.52k_0 \pm 0.02k_0$	$k_{xy}(3) = 2.4k_0 \pm 0.05k_0$	$\sim 0.6k_0 \pm 0.04k_0$
	Inner two modes, $N = 2$	$k_d(2) = 1.51k_0 \pm 0.03k_0$		$k_{xy}(2) = 1k_0 \pm 0.05k_0$	
	Innermost fractional modes, $N = 1$	$k_d(1) = 0.74k_0 \pm 0.04k_0$		$k_{xy}(1) = 0.22k_0 \pm 0.04k_0$	

$k_{xy}(N) = k_d(N) - k_u(N)$. The bulk thermal conductance measured with the gate fully open is $k_{\text{bulk}} \sim 0.54k_0 \pm 0.03k_0$ [Fig. 3(b)]. Interestingly, we find a half-integer value, $k_{xy}(3) = 2.5k_0 \pm 0.07k_0$, with SG fully pinched [Fig. 3(c)]. However, upon removing the outer integer edges, k_{xy} (for $N = 1, 2$) deviates from half-integer values (see Table I). Unlike at $\nu = 2$, here, k_{xy} decreases by $\sim 1.1k_0$ (instead of $1k_0$) when the integer edge modes are removed, suggesting a greater energy loss of the inner modes when isolated. We will return to this issue later.

For the second even-denominator $\nu = 7/2$ state, we have measured a different device with an L to R distance of 30 μm and showing improved quality of the state [refer to Supplemental Material [46], Figs. 1(e) and 1(f)]. The J_{down} (or J_{up}) vs $T_L^2 - T_0^2$ (or $T_R^2 - T_0^2$) plots corresponding to this state are presented in Supplemental Material-6 [46]. Table I also summarizes the thermal conductance coefficients determined from these plots. Similar to $\nu = 5/2$, here, we once again observe a half-integer value, $k_{xy}(4) = 3.48k_0 \pm 0.07k_0$, with SG fully pinched and deviations from half-integer values with the outer edge modes removed. Note that the $\nu = 7/2$ state has an extra integer mode compared to the $\nu = 5/2$ state. However, unlike at $\nu = 5/2$ we observe identical bulk and upstream thermal conductances: $k_{\text{bulk}} = 0.6k_0 \pm 0.04k_0$ and $k_u \sim 0.52k_0 \pm 0.02k_0$ (used to calculate k_{xy}). Note that k_{bulk} is measured with SG fully opened, while k_u is measured with the SG closed, either fully or partially. Thus, the observed identical values indicate complete heat loss from the upstream edges, consistent with the device's longer floating contact separation (30 μm).

The observed half-integer k_{xy} values for fully closed SG align with the PH-Pf order. In Supplemental Material-7 [46], we compare the measured k_{xy} for different numbers of edge modes with the expected values for the PH-Pf order. The comparison shows a lower than expected k_{xy} of the most inner channel when the integer modes are peeled away for both the studied states. It is crucial to note that while the measurement of k_{2t} relies on the heat that leaves the heated source contact, our present measurement of k_d or k_u depends on the heat that reaches the contact R (or, alternatively, the contact L), which may suffer from heat loss on its way (after emanating from the heated contact). We find that the measured upstream heat conductance k_u is independent of gate voltage (refer to Supplemental Material-5 [46]), suggesting constant heat loss (possibly to the bulk). Consequently, the observed deviation in k_{xy} indicates increased heat loss from the inner downstream charged modes. We suggest that as we peel off the integer modes by "opening" the SG gate, the confining potential gets softer, leading to a low drift velocity of the edge modes and thus increasing its heat loss. Additionally, partial equilibration among all modes in the ungated etched regions, each ∼2 μm long, between SG and each floating contact can alter the total heat transported by the edge modes propagating along the partially closed gate. This might also lead to unequal heat losses in the upstream and downstream directions, thus contributing to the deviation in k_{xy} in these conditions. These handicaps were considered in future designs with shorter etched regions.

Conclusion—This rather elaborate measurement configuration was developed to obtain the topological order of the states in the FQH regime [42,43]. This method overcomes the drawback of previously tested two-terminal measurements (the possible lack of full thermal equilibration) [21,22,24]. It allows employing higher-quality 2DEG (with wider conductance plateaus and lower longitudinal resistance) by eliminating the contribution to heat transfer of the highly intricate doping configuration [21,42,44,45]. While the long-standing theoretical prediction of the order of the even-denominator states is the A-Pf order [3–5], all our measurements indicate the PH-Pf order [21–23]. Finding the same order in the two even-denominator states may point to a more fundamental reason for the consistent finding of the PH-Pf order. It will be commendable if new theoretical works address the unavoidable disorder and Landau-level mixing in the GaAs devices [8–10,49,50]. These shortfalls might be overcome in high-quality hBN-encapsulated graphene hosting even-denominator states [51].

Acknowledgment—We thank Dima E. Feldman for the fruitful discussions. We also thank Sourav Manna and Ankur Das for the valuable discussions and suggestions. M. H. acknowledges the support of the European Research Council under the European Union's Horizon 2020 research and innovation program (Grant Agreement No. 833078).

A. K. P. and P. T. contributed equally to this letter.

[1] R. Willett, J. P. Eisenstein, H. L. Störmer, D. C. Tsui, A. C. Gossard, and J. H. English, Observation of an even-denominator quantum number in the fractional quantum Hall effect, Phys. Rev. Lett. **59**, 1776 (1987).
[2] G. Moore and N. Read, Non-Abelions in the fractional quantum Hall effect, Nucl. Phys. **B360**, 362 (1991).
[3] R. H. Morf, Transition from quantum Hall to compressible states in the second Landau level: New light on the $\nu = 5/2$ enigma, Phys. Rev. Lett. **80**, 1505 (1998).
[4] M. Levin, B. I. Halperin, and B. Rosenow, Particle-hole symmetry and the Pfaffian state, Phys. Rev. Lett. **99**, 236806 (2007).
[5] S.-S. Lee, S. Ryu, C. Nayak, and M. P. A. Fisher, Particle-hole symmetry and the $\nu = 5/2$ quantum Hall state, Phys. Rev. Lett. **99**, 236807 (2007).
[6] C. Nayak, S. H. Simon, A. Stern, M. Freedman, and S. Das Sarma, Non-Abelian anyons and topological quantum computation, Rev. Mod. Phys. **80**, 1083 (2008).
[7] A. Stern, Non-Abelian states of matter, Nature (London) **464**, 187 (2010).
[8] M. Storni, R. H. Morf, and S. Das Sarma, Fractional quantum Hall state at $\nu = 5$ 2 and the Moore-Read Pfaffian, Phys. Rev. Lett. **104**, 076803 (2010).
[9] A. Wójs, C. Tőke, and J. K. Jain, Landau-level mixing and the emergence of Pfaffian excitations for the 5/2 fractional quantum Hall effect, Phys. Rev. Lett. **105**, 096802 (2010).
[10] P. T. Zucker and D. E. Feldman, Stabilization of the particle-hole Pfaffian order by Landau-level mixing and impurities that break particle-hole symmetry, Phys. Rev. Lett. **117**, 096802 (2016).
[11] E. H. Rezayi, Landau level mixing and the ground state of the $\nu = 5/2$ quantum Hall effect, Phys. Rev. Lett. **119**, 026801 (2017).
[12] L. Antonić, J. Vučičević, and M. V. Milovanović, Paired states at 5/2: Particle-hole Pfaffian and particle-hole symmetry breaking, Phys. Rev. B **98**, 115107 (2018).
[13] W. Pan, R. R. Du, H. L. Stormer, D. C. Tsui, L. N. Pfeiffer, K. W. Baldwin, and K. W. West, Strongly anisotropic electronic transport at Landau level filling factor $\nu = 9/2$ and $\nu = 5/2$ under a tilted magnetic field, Phys. Rev. Lett. **83**, 820 (1999).
[14] R. L. Willett, L. N. Pfeiffer, and K. West, Measurement of filling factor 5/2 quasiparticle interference with observation of charge e/4 and e/2 period oscillations, Proc. Natl. Acad. Sci. U.S.A. **106**, 8853 (2009).
[15] Y. Liu, J. Shabani, D. Kamburov, M. Shayegan, L. N. Pfeiffer, K. W. West, and K. W. Baldwin, Evolution of the 7/2 fractional quantum Hall state in two-subband systems, Phys. Rev. Lett. **107**, 266802 (2011).
[16] D. E. Feldman and B. I. Halperin, Fractional charge and fractional statistics in the quantum Hall effects, Rep. Prog. Phys. **84**, 076501 (2021).
[17] R. L. Willett, K. Shtengel, C. Nayak, L. N. Pfeiffer, Y. J. Chung, M. L. Peabody, K. W. Baldwin, and K. W. West, Interference measurements of non-Abelian e/4 & Abelian e/2 quasiparticle braiding, Phys. Rev. X **13**, 011028 (2023).
[18] I. P. Radu, J. Miller, C. Marcus, M. Kastner, L. Pfeiffer, and K. West, Quasi-particle properties from tunneling in the v= 5/2 fractional quantum Hall state, Science **320**, 899 (2008).
[19] X. Lin, C. Dillard, M. A. Kastner, L. N. Pfeiffer, and K. W. West, Measurements of quasiparticle tunneling in the $\upsilon = 5$ 2 fractional quantum Hall state, Phys. Rev. B **85**, 165321 (2012).
[20] S. Baer, C. Rössler, T. Ihn, K. Ensslin, C. Reichl, and W. Wegscheider, Experimental probe of topological orders and edge excitations in the second Landau level, Phys. Rev. B **90**, 075403 (2014).
[21] M. Banerjee, M. Heiblum, V. Umansky, D. E. Feldman, Y. Oreg, and A. Stern, Observation of half-integer thermal Hall conductance, Nature (London) **559**, 205 (2018).
[22] B. Dutta, V. Umansky, M. Banerjee, and M. Heiblum, Isolated ballistic non-Abelian interface channel, Science **377**, 1198 (2022).
[23] B. Dutta, W. Yang, R. Melcer, H. K. Kundu, M. Heiblum, V. Umansky, Y. Oreg, A. Stern, and D. Mross, Distinguishing between non-Abelian topological orders in a quantum Hall system, Science **375**, 193 (2022).
[24] S. Jezouin, F. Parmentier, A. Anthore, U. Gennser, A. Cavanna, Y. Jin, and F. Pierre, Quantum limit of heat flow across a single electronic channel, Science **342**, 601 (2013).
[25] S. K. Srivastav, M. R. Sahu, K. Watanabe, T. Taniguchi, S. Banerjee, and A. Das, Universal quantized thermal conductance in graphene, Sci. Adv. **5**, eaaw5798 (2019).
[26] C. L. Kane and M. P. A. Fisher, Quantized thermal transport in the fractional quantum Hall effect, Phys. Rev. B **55**, 15832 (1997).
[27] A. Cappelli, M. Huerta, and G. R. Zemba, Thermal transport in chiral conformal theories and hierarchical quantum Hall states, Nucl. Phys. **B636**, 568 (2002).
[28] S. K. Srivastav, R. Kumar, C. Spånslätt, K. Watanabe, T. Taniguchi, A. D. Mirlin, Y. Gefen, and A. Das, Vanishing thermal equilibration for hole-conjugate fractional quantum Hall states in graphene, Phys. Rev. Lett. **126**, 216803 (2021).
[29] S. K. Srivastav, R. Kumar, C. Spånslätt, K. Watanabe, T. Taniguchi, A. D. Mirlin, Y. Gefen, and A. Das, Determination of topological edge quantum numbers of fractional quantum Hall phases by thermal conductance measurements, Nat. Commun. **13**, 5185 (2022).
[30] K. Nomura, S. Ryu, A. Furusaki, and N. Nagaosa, Cross-correlated responses of topological superconductors and superfluids, Phys. Rev. Lett. **108**, 026802 (2012).
[31] H. Sumiyoshi and S. Fujimoto, Quantum thermal Hall effect in a time-reversal-symmetry-broken topological superconductor in two dimensions: Approach from bulk calculations, J. Phys. Soc. Jpn. **82**, 023602 (2013).

[32] S.-H. Do, S.-Y. Park, J. Yoshitake, J. Nasu, Y. Motome, Y. S. Kwon, D. Adroja, D. Voneshen, K. Kim, T.-H. Jang *et al.*, Majorana fermions in the Kitaev quantum spin system α-RuCl3, Nat. Phys. **13**, 1079 (2017).

[33] Y. Kasahara, T. Ohnishi, Y. Mizukami, O. Tanaka, S. Ma, K. Sugii, N. Kurita, H. Tanaka, J. Nasu, Y. Motome *et al.*, Majorana quantization and half-integer thermal quantum Hall effect in a Kitaev spin liquid, Nature (London) **559**, 227 (2018).

[34] T. Yokoi, S. Ma, Y. Kasahara, S. Kasahara, T. Shibauchi, N. Kurita, H. Tanaka, J. Nasu, Y. Motome, C. Hickey *et al.*, Half-integer quantized anomalous thermal Hall effect in the Kitaev material candidate α-$RuCl_3$, Science **373**, 568 (2021).

[35] N. Read and D. Green, Paired states of fermions in two dimensions with breaking of parity and time-reversal symmetries and the fractional quantum Hall effect, Phys. Rev. B **61**, 10267 (2000).

[36] S. H. Simon, M. Ippoliti, M. P. Zaletel, and E. H. Rezayi, Energetics of Pfaffian–anti-Pfaffian domains, Phys. Rev. B **101**, 041302(R) (2020).

[37] S. H. Simon, Interpretation of thermal conductance of the $\nu = 5/2$ edge, Phys. Rev. B **97**, 121406(R) (2018).

[38] D. E. Feldman, Comment on "interpretation of thermal conductance of the $\nu = 5/2$ edge", Phys. Rev. B **98**, 167401 (2018).

[39] S. H. Simon and B. Rosenow, Partial equilibration of the anti-Pfaffian edge due to Majorana disorder, Phys. Rev. Lett. **124**, 126801 (2020).

[40] M. Hein and C. Spånslätt, Thermal conductance and noise of Majorana modes along interfaced $\nu = 5$ 2 fractional quantum Hall states, Phys. Rev. B **107**, 245301 (2023).

[41] S. Manna, A. Das, M. Goldstein, and Y. Gefen, Full classification of transport on an equilibrated $5/2$ edge, Phys. Rev. Lett. **132**, 136502 (2024).

[42] R. A. Melcer, S. Konyzheva, M. Heiblum, and V. Umansky, Direct determination of the topological thermal conductance via local power measurement, Nat. Phys. **19**, 327 (2023).

[43] R. A. Melcer, A. Gil, A. K. Paul, P. Tiwari, V. Umansky, M. Heiblum, Y. Oreg, A. Stern, and E. Berg, Heat conductance of the quantum Hall bulk, Nature (London) **625**, 489 (2024).

[44] V. Umansky, M. Heiblum, Y. Levinson, J. Smet, J. Nübler, and M. Dolev, Mbe growth of ultra-low disorder 2 deg with mobility exceeding 35×106 cm2/v s, J. Cryst. Growth **311**, 1658 (2009).

[45] V. Y. Umansky and M. Heiblum, Mbe growth of high-mobility 2 deg, in *Molecular Beam Epitaxy: From Research to Mass Production* (Elsevier Science, New York, 2013), pp. 121–137.

[46] See Supplemental Material at http://link.aps.org/supplemental/10.1103/PhysRevLett.133.076601 for detailed device structure, conductance and thermal noise measurement methods, and additional data.

[47] A. O. Slobodeniuk, I. P. Levkivskyi, and E. V. Sukhorukov, Equilibration of quantum Hall edge states by an Ohmic contact, Phys. Rev. B **88**, 165307 (2013).

[48] E. Sivre, A. Anthore, F. Parmentier, A. Cavanna, U. Gennser, A. Ouerghi, Y. Jin, and F. Pierre, Heat Coulomb blockade of one ballistic channel, Nat. Phys. **14**, 145 (2018).

[49] S. Das, S. Das, and S. S. Mandal, Anomalous reentrant $5/2$ quantum Hall phase at moderate Landau-level-mixing strength, Phys. Rev. Lett. **131**, 056202 (2023).

[50] L. Herviou and F. Mila, Possible restoration of particle-hole symmetry in the $5/2$-quantized Hall state at small magnetic field, Phys. Rev. B **107**, 115137 (2023).

[51] K. Huang, H. Fu, D. R. Hickey, N. Alem, X. Lin, K. Watanabe, T. Taniguchi, and J. Zhu, Valley isospin controlled fractional quantum Hall states in bilayer graphene, Phys. Rev. X **12**, 031019 (2022).